CCFE
CULHAM CENTRE FOR FUSION ENERGY

UK Atomic Energy Authority

UKAEA-CCFE-PR(23)134

R. Thomas, Ö. Koç, T. Ungar, G. Zilahi, H. Xu, Z. Hegedues, U. Lienert, G. Ribarik, H. Sharma, P. Kenesei, M. Preuss, P. Frankel

Characterisation of irradiation damage using x-ray diffraction line profile analysis

Characterisation of irradiation damage using x-ray diffraction line profile analysis

R. Thomas, Ö. Koç, T. Ungar, G. Zilahi, H. Xu, Z. Hegedues, U. Lienert, G. Ribarik, H. Sharma, P. Kenesei, M. Preuss, P. Frankel

This is a preprint of a paper submitted for publication in
ASTM Zirconium in the Nuclear industry conference proceedings

Characterisation of irradiation damage using x-ray diffraction line profile analysis

R. Thomas[1*], O. Koc[1], T. Ungár[1,4], G. Zilahi[2], Z. Hegedues[3], U. Lienert[3], G. Ribarik[4], H. Sharma[5], P. Kenesei[5], M. Preuss[1,6], P. Frankel[1]

*** rhys.thomas@manchester.ac.uk**

[1] Department of Materials, The University of Manchester, Oxford Road, Manchester, M13 9PL, UK.

[2] United Kingdom Atomic Energy Authority, Culham Science Centre, Abingdon, Oxon, OX14 3DB, UK.

[3] Deutsches Elektronen-Synchrotron (DESY), Hamburg, Germany

[4] Department of Materials Physics, Eötvös University Budapest, Hungary

[5] Advanced Photon Source, Argonne National Laboratory, Lemont, IL, USA

[6] Department of Materials Science and Engineering, Monash University, Clayton, VIC 3800, Australia.

Abstract

During operation, structural components made of zirconium alloys are subject to neutron irradiation, which leads to the displacement of zirconium atoms from their lattice sites, the production of self-interstitials and vacancies, and eventually dislocation loops. This process can lead to deleterious effects such as irradiation growth, creep and embrittlement as well as accelerated aqueous corrosion.

Quantitative analysis of dislocation line densities is seen as an important pathway to distinguish between the irradiation response of different alloys. Analysis of irradiation damage using x-ray diffraction (XRD) line profile analysis has proven to be a powerful complementary technique to transmission electron microscope (TEM), which samples a comparatively large volume and is less affected by the subjectivity of image analysis.

In the present work, we present 3 different types of x-ray diffraction experiments and their analysis, describe their purpose and the new insight achieved using such techniques. First, we present work carried out on neutron irradiated samples, comparing dislocation line densities measured by XRD with macroscopic growth measurements. Here we demonstrate a correlation between <c>-loop dislocation density and irradiation induced growth strain. A second experiment using a synchrotron-based x-ray microbeam enabled the mapping of dislocation line densities as a function of depth from the surface of proton irradiated Zr-alloys. These data are compared with calculated damage profiles providing new insight in possible early saturation of damage. Finally, the last example presented here focuses on synchrotron-based 3D-XRD measurements where dislocation loop line densities were analysed in hundreds of individual grains providing excellent statistics about the grain-to-grain variability of line densities.

Keywords

Zirconium, Irradiation, XRD, Line Profile Analysis

1. Introduction

Quantifying the relationship between dose and irradiation damage during the life of a zirconium alloy component is important for gaining an understanding of potential subsequent degradation mechanisms such as irradiation induced growth and irradiation hardening. Although small changes in composition have yielded significant improvements in performance in the past, particularly on corrosion and growth during irradiation, the root cause for such improvements are still poorly understood constraining the translation of such improvements in higher fuel burn-up.

Characterisation of irradiation induced dislocation loop structure is typically carried out in a transmission electron microscope (TEM), where dislocation loops can be seen; counted; their size, shape and spacing, Burgers vector and habit plane measured and interstitial or vacancy character determined [1,2]. Line profile analysis (LPA) of an x-ray diffraction (XRD) pattern is a method which can yield complementary information. Recently, the Convolutional Multiple Whole Profile (CMWP) software has been upgraded to measure the dislocation density of irradiation-induced dislocation loops in zirconium alloys [3]. The technique has now been extensively used to measure the dislocation density of <a>- and <c>-loops in proton- and neutron-irradiated zirconium alloys, investigating the effect of irradiation dose [4], irradiation temperature [2], thermal stability [5], loop size [6], satellite peaks [3] and deformation [7].

TEM is still essential however as LPA requires contrast factors to be calculated based on the Burgers vector, shape and habit plane of the dislocation structures. The strain field of such structures must be determined or modelled, and the accuracy of the dislocation density measured by CMWP relies on the accuracy of this calculation. Loops of size on the order of nanometres and larger contribute to peak broadening [8]. The short-range strain field of point defects and smaller defect clusters cause diffuse scattering below the Bragg peaks which therefore is not currently considered by CMWP. There is also an upper limit to the measurement of coherently diffracting crystallite size of ~ 2 μm since size broadening becomes negligible beyond this size and a lower limit to the measurement of dislocation density of $\sim 0.01 \times 10^{14}$ m^{-2}.

Proton irradiation is routinely used as a surrogate for neutron irradiation, since proton irradiated samples are less active and are therefore easier to handle. Protons only

penetrate a relatively short distance, leaving only a thin damaged layer on the surface of the sample with a variable dose profile. In the case of 2 MeV protons and irradiating Zr, this layer is around 30 μm thick. A variable dose profile in this layer could be exploited to investigate multiple doses and dose rates in a single sample and this will be demonstrated here to allow for systematic studies of loop evolution. Other important considerations remain, such as the choice of conversion factor between neutron fast fluence (E > 1 MeV) and dpa, which is generally thought to be 3 – 7 $\times 10^{24}$ n/m^2 per dpa depending on reactor and neutron energy profile [9,10]. The effect of crystal orientation relative to irradiation direction, also known as channelling [11], is also not well understood.

First, experiments performed using laboratory XRD to quantify irradiation damage in neutron irradiated coupons will be summarised. Using a synchrotron microbeam, the depth profile of dislocation density and arrangement parameter in a proton irradiated sample will be investigated. Finally, grain resolved experiments were used to determine loop type, dislocation density spread and orientation dependence of dislocation density in a proton irradiated sample.

2. Experimental Method

2.1. Material

The material studied here came from various sources. Bulk measurements were performed neutron-irradiated Zircaloy-2 and low-Sn ZIRLO, which came from a Nuclear Fuel Industry Research (NFIR) led irradiation campaign carried out at the BOR-60 reactor. The neutron fast fluences (E > 1MeV) studied are 2.1, 8.2 and 16.2 $\times 10^{24}$ n/m^2, irradiated at 320 °C. More details about these irradiated specimens can be found in [12]. Summaries of the material, including alloy compositions, are given in Table 2. The conversion between neutron fluence and dpa is given as 5 $\times 10^{24}$ n/m^2 per dpa, based on the BOR-60 neutron energy spectrum [10,12,13]. The average damage rate in the BOR-60 reactor is 8.9 $\times 10^{-7}$ dpa/s, however both axial and cycle-to-cycle variations occurred [10]. Since irradiation growth has a strong texture dependence, the Kearns factors for each material are compared in Table 1, which shows both materials have a very similar texture.

Table 1. Kearns factors for Zircaloy-2 RXA and low-Sn ZIRLO RXA.

	Pole	$\mathbf{f_{radial}}$	$\mathbf{f_{circum.}}$	$\mathbf{f_{axial}}$
Zircaloy-2 RXA	Basal	0.659	0.262	0.079
	Prism	0.158	0.378	0.464
Low-Sn ZIRLO RXA	Basal	0.689	0.232	0.079
	Prism	0.152	0.388	0.460

Recording diffraction patterns at different depths of a sample (depth-profiling) was carried out on Zircaloy-4 irradiated with 2 MeV protons, at 350 °C, to nominal doses (about 18 μm from the surface) of 0.1, 0.5, 1.0 and 2.0 dpa, at the Dalton Cumbrian Facility, with a dose rate of 1.4 $\times 10^{-5}$ dpa/s for that particular position. The irradiated area and current remained constant, therefore irradiation times were 1.6, 8, 16 and 32 hours for each sample respectively. Grain resolved measurements with 3D-LPA were carried out on Zr-0.1Fe irradiated with 2 MeV protons to nominal doses of 0.8 and 3.0 dpa at 350 °C at the Michigan Ion Beam Laboratory at a dose rate of 1.3 $\times 10^{-5}$ dpa/s. Prior to irradiation, the surface to be irradiated was mechanically polished with a final colloidal silica step to achieve an EBSD quality finish.

Table 2. Summary of material parameters and irradiation conditions, for the three experiment types.

Experiment	**Alloy**	**Composition (wt%)**	**Species and dose (dpa)**	**Dose rate (dpa/s)**	**Irradiation temp. (°C)**
Bulk	Low-Sn ZIRLO RXA	Zr-0.95Nb-0.66Sn-0.12Fe-0.12O	Neutrons to 4.2, 11.2, 16.4, 22.2, 32.4	8.9 $\times 10^{-7}$	320
	Zircaloy-2 RXA	Zr-1.35Sn-0.17Fe-0.10Cr- 0.07Ni-0.12O			320
Depth profiling	Zircaloy-4 RXA	Zr-0.17Fe-1.24Sn-0.10Cr	Protons to 0.1, 0.5, 1.0, 2.0	1.4 $\times 10^{-5}$	350
Grain resolved	Zr-0.1Fe	Zr-0.1Fe	Protons to 0.8, 3.0	1.3 $\times 10^{-5}$	350

Different sample geometries are required for each different type of experiment. For laboratory-based bulk experiments, which are performed in reflection, a sample allowing a large beam footprint is preferrable, but a beam size of down to 0.1 mm can be used with a corresponding reduction in intensity and increase in collection time. An

example of a typical BOR-60 coupon for XRD-LPA analysis is shown in Figure 1 (a). Both sides of the sample were electropolished with a 25% perchloric acid and 75% acetic acid solution to remove any surface deformed layer.

For depth profiling, (0.5 x 1 x 5) mm cross-sections of proton irradiated material were prepared by cutting, grinding and polishing, as shown in Figure 1 (b). The total thickness probed by x-rays is 0.5 mm, which allows sufficient diffraction signal to be captured at high energy synchrotron beamlines, whilst sampling enough grains to ensure the signal is not too spotty.

For 3D-LPA, around 300-400 grains should be visible in each diffraction 2D image to reduce the chance of overlap between diffraction spots of individual grains. Since the grain size of zirconium alloys is around 10 μm, samples were prepared by focussed ion beam at room temperature, as shown in Figure 1 (c). A tapered geometry was chosen, with two discrete regions, one with thickness 15 μm and one with thickness 30 μm from the proton irradiated surface.

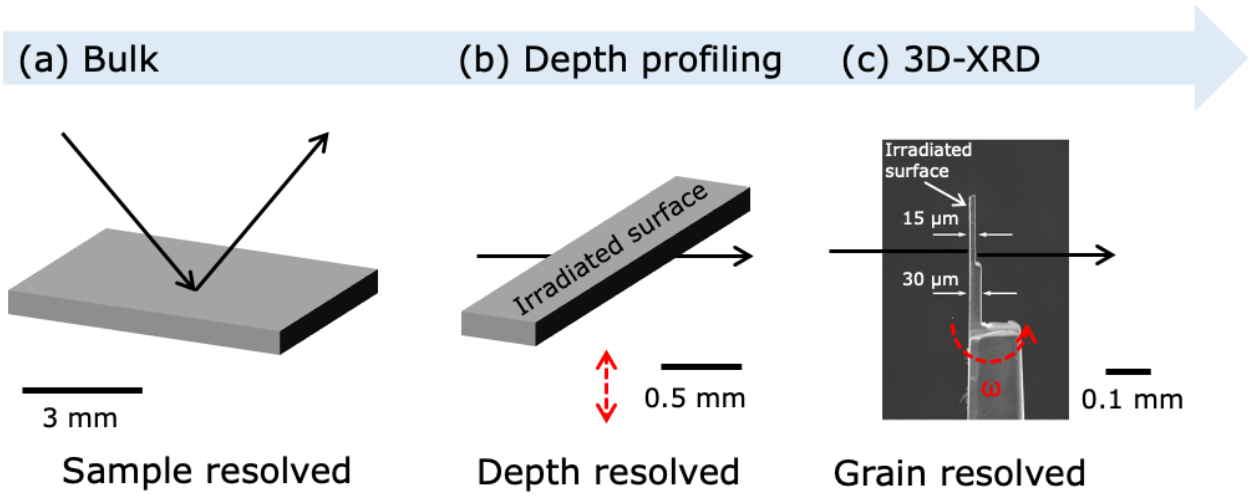

Figure 1. Comparison of sample geometry for (a) laboratory bulk XRD sample resolved measurements, (b) synchrotron microbeam depth resolved measurements and (c) synchrotron grain resolved measurement. Black arrows illustrate the incident and diffracted beams, which is reflected in (a) and transmitted in (b) and (c). Red arrow shows movement of sample during scanning. The irradiated surface is also shown, assuming a proton-irradiated sample.

2.2. SRIM

The Stopping Range of Ions in Matter (SRIM) software was used to predict the dose profile as a function of depth for proton irradiated samples [14,15]. As recommended by Stoller et al [14], a quick Kinchin-Pease calculation is used and the lattice binding energy was set to 0 eV. The threshold displacement energy was set to 40 eV as recommended by ASTM [16]. The total number of vacancies generated is calculated and output as a function of sample depth. Multiplication by fluence and division by number density then gives the number of displacements per atom (dpa). Predicted dose and H implantation as a function of depth is shown Figure 2 for 2 MeV protons which is relevant to all proton irradiations in this paper. Since the energy loss of a proton is proportional to the inverse square of velocity, the peak in damage occurs near the end of the proton's trajectory, also known as the Bragg peak. The nominal dose was calculated at 60% of the depth to the Bragg peak, i.e. around 18 μm from the surface.

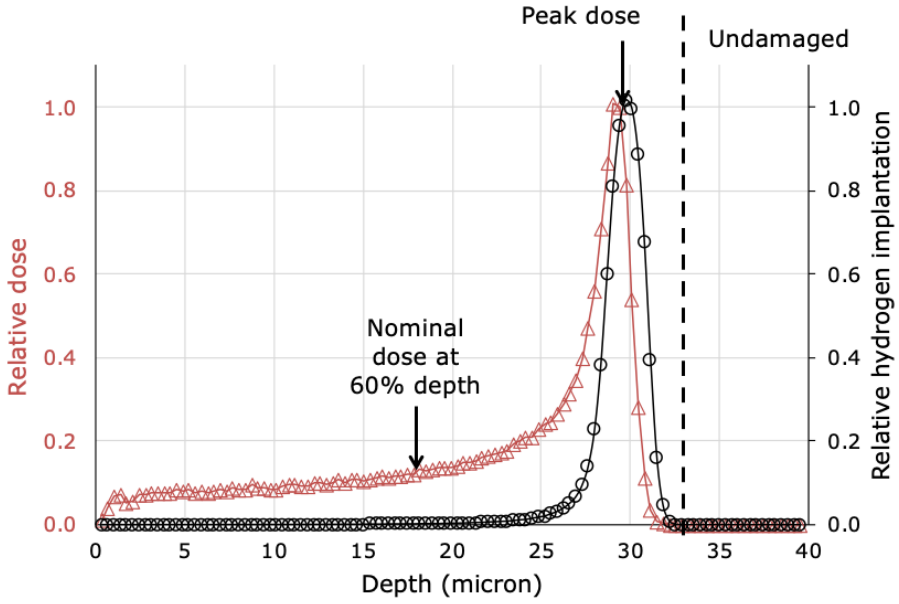

Figure 2. Relative dose (triangles) and relative hydrogen ion implantation (circles) as a function of penetration depth for 2 MeV protons in zirconium alloys.

2.3. XRD

Bulk X-ray diffraction was undertaken using two instruments, a Rigaku SmartLab rotating anode diffractometer located at the Materials Research Facility, CCFE and a

Rigaku SmartLab sealed x-ray tube diffractometer located at the University of Manchester. Multiple measurements were taken of both sides of each sample, using both diffractometers. Both diffractometers used a Hypix-3000(H) (77.5 mm active length) 2D-detector (mounted vertically) operating in 2D mode in theta-omega geometry employing a Copper Line Focus X-ray tube with parallel beam selection from the Rigaku Cross Beam Optic (CBO) to the Rigaku Ge(220)x2 optic producing monochromatic $K\alpha_1$ radiation ($K\alpha_1$=1.540598 Å).

A custom incident double slit holder (GHM) matched to the incident beam mask of 2 mm and programmable incidence slit 0.5 mm were used. Data collection were undertaken over an angular range from 28 to 114° coupled theta/2theta at 0.02° step, with a total acquisition time per sample of 24 hours. Integration was carried out over an angular range from 178 to 182° in eta, the azimuthal angle around the diffraction rings captured on the 2D detector.

Depth profiling experiments were carried out at the P21.2 beamline at the PETRA III synchrotron facility at DESY in Hamburg, Germany, with a beam energy of 65 keV and a sample - 2D detector distance of 0.9 m, as illustrated in Figure 3 (a). A spot size of (2 x 2) μm was used and the sample was scanned from the surface to 40 μm beneath the proton irradiated surface by moving the stage in increments of 2 μm. The sample was translated perpendicular to the scanning direction by around 200 μm during each scan to improve grain statistics and therefore reduce the spottiness of the pattern. Only a small subset of grains will have crystallographic planes in a diffracting condition for a given reflection in the profile. The grain-to-grain variability of dislocation density will be investigated later. The precise location of the sample edge is important to determine, such that the measurements can be compared with predicted dose from SRIM. The position of the edge was determined from the change in beam intensity measured at the beam stop, which is higher when the beam is going through air, compared to being attenuated by the sample. This was also used to align the sample, since the transition between air and sample becomes sharper when the sample edge is parallel to the beam.

Grain resolved dislocation density measurement was carried out at the 1-ID beamline of the Argonne Photon Source (APS) synchrotron, with a beam energy of 61.33 keV and a line focused beam of width 1 mm and height 40 μm. Samples were mounted in a goniometer for incremental rotation 0.25° around the ω angle from -180° to +180°, as

illustrated in in Figure 3 (b). Two sets of scans were carried out, one on the 15 µm thick region of the sample and another on the 30 µm thick region. Three sets of detectors were used, a single 'close' detector at 20 mm away from the sample, a single 'medium' detector at 500 mm away from the sample and a 2x2 array of detectors 4 m away from the sample, as illustrated in Figure 3 (b).

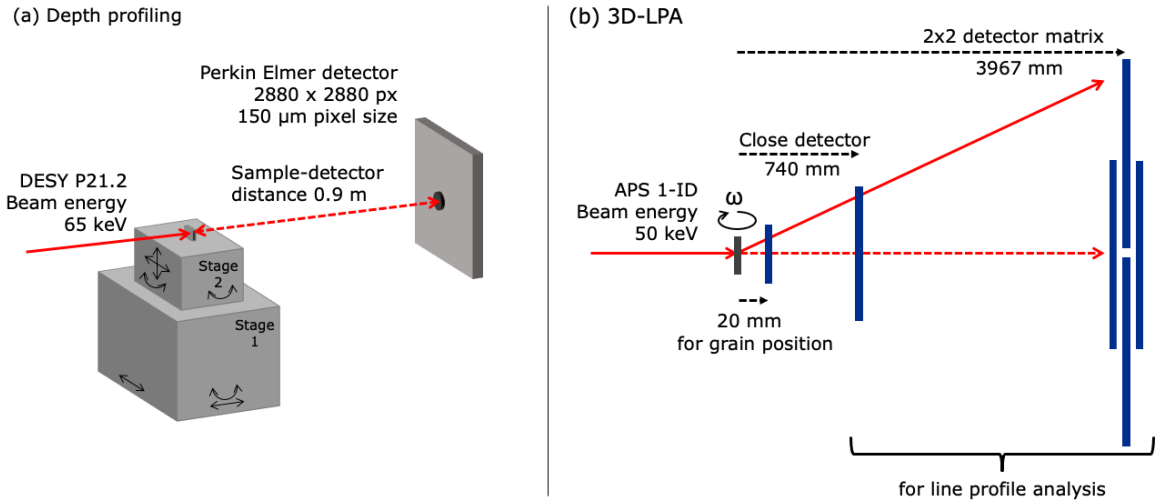

Figure 3. Experimental arrangement for (a) depth profiling at DESY and (b) 3D-LPA at APS.

Following data collection, the diffraction peaks in each of the frames from the middle detector were identified and filtered. Given enough ω frames and reflection positions are captured, certain groups of diffraction peaks can be indexed into grains. The groups of diffraction peaks corresponding to each grain were projected from the close detector, to the far detectors, which have higher angular resolution. Integration was carried out to generate a diffraction pattern for each grain from the far detectors. The technique is described in more detail in [17].

As the sample was rotated around 360°, there is no limitation on the orientation of the grains that can be detected. There is a small fraction of crystal planes that never turn into reflection orientation because their normal is almost parallel to the rotation axis, but grains can be indexed based on their other reflections. The only limitation is the detection limit of the peaks, i.e., small grains that don't have strong enough reflections. The texture of the material studied, relative to the direction of interest (the irradiation direction), will govern the grain orientations sampled. Since the irradiation was along

the normal direction, ~ 90% of grains have their <c>-axis within 50 degrees of the irradiation direction.

2.4. Line profile analysis

Diffraction peak profiles broaden fundamentally due to size and strain effects [18]. Line profile analysis is a technique used to quantify these effects, to obtain physical microstructural parameters such as crystallite size and dislocation density. In the current study, line profile analysis was carried out using the Convolutional Multiple Whole Profile (CMWP) method [19,20], which is based on fitting of measured diffraction profiles with theoretical physical profile functions that describe the strain fields and morphology of different lattice defects and their impact on diffraction peak broadening [21,22].

Profiles related to the different peak broadening effects convolute in the diffraction patterns. Consequently, CMWP convolutes all calculated peak profiles to obtain a theoretical profile. 1) Instrumental effects are taken into account by measuring a reference sample (LaB_6 in the lab and CeO_2 at the synchrotron in the current study), from which CMWP creates an instrumental profile. 2) The size profile is calculated by assuming a log-normal size distribution of coherently scattering domains [19,20]. 3) The Fourier transform of strain profiles can be given as [18]:

$$A_{hkl}^{S}(L) \cong \exp[-2\pi^2 g^2 L^2 \langle \varepsilon_{g,L}^2 \rangle] \,, \qquad (2)$$

where g is the absolute value of the diffraction vector and L is the Fourier variable. For dislocations, the mean square strain, $\langle \varepsilon_{g,L}^2 \rangle$ was developed by Krivoglaz [21] and Wilkens [22]:

$$\langle \varepsilon_{g,L}^2 \rangle \cong \frac{\rho C b^2}{4\pi} f(\eta), \qquad (3)$$

where ρ and b are the density and the Burgers vector of dislocations, C is the dislocation contrast factor, $\eta = L/R_e$, and R_e is the effective outer cut-off radius of dislocations. Since R_e depends on the dislocation densities, sometimes it is useful to use the dimensionless parameter $M = R_e\sqrt{\rho}$ describing the arrangement or the dipole

character of dislocations [3]. Smaller or larger *M* values indicate stronger or weaker dipole character.

When characterizing dislocation loops in irradiated Zr the contrast factors of dislocations play an important role [3]. For dislocation loops in irradiated Zr, contrast factors were calculated by Balogh et al. [8] for a variety of ellipticities. In the current study, loops are assumed to be circular (ellipticity 1). The partial dislocation densities of <*a*>- and <*c*>- loops can then be determined by splitting the means square strain. More details about this procedure can be found in [23]. The uncertainties quoted on the values of physical parameters are calculated during the Monte Carlo optimisation procedure and more details can be found in [24].

3. Results

Bulk measurement of BOR-60 samples

Typical diffraction patterns are shown in Figure 4, for both a non-irradiated and a neutron-irradiated Zircaloy-2 sample at a fluence of 16.2 $\times 10^{25}$ n/m^2 (32.4 dpa). The experimental data is shown in black and the fitted profile generated by CMWP, for which the physical parameters are known, are shown in red. These two profiles match well for both the non-irradiated and neutron irradiated cases, suggesting the CMWP method worked well and has accounted for the experimentally measured features in the line profile. Qualitatively, the neutron-irradiated pattern shows significant broadening of all peaks, compared to the non-irradiated pattern, suggesting the presence of <a>- and <c>-loops.

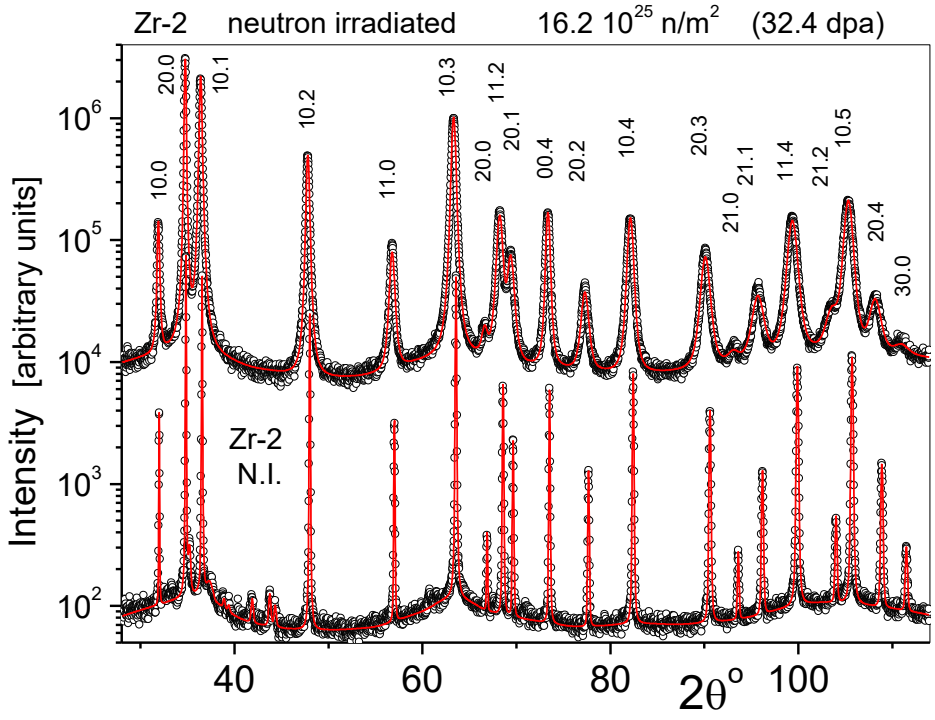

Figure 4. Measured (open circles) and CMWP calculated (red line) diffraction patterns of the non-irradiated (N.I.) and the neutron irradiated to the fluence of 16.2×10²⁵ n/m² (32.4 dpa) patterns of Zircaloy-2 BOR-60 specimens.

The Williamson-Hall (WH) and the modified Williamson-Hall (mWH) plots of the integral breadths (β) are shown in Figure 5 (a) and (b), respectively. The large, almost anti-coincidental, variation of β *vs*. K in the WH plot is partially related to the elastic anisotropy of Zr, however, mainly due to the alignment of <a> and <c> loop Burgers vectors in specific, almost orthogonal, directions. The variation of β in Fig. 5a is rationalized in the mWH plot by taking the contrast factors for <a>- and <c>- loops for each reflection into account in replacing K by $K\sqrt{C}$. The gradients and intercepts of the linear regressions through the β values are proportional to dislocation density and crystallite size showing that the contrast factors for <a> and <c> loops calculated by Balogh et al. [8] are reasonable. The zero intercepts indicate that the crystallite size is larger than about 1 μm in line with TEM or EBSD observations that loops do not tilt the lattice planes. The substantially larger slope for <a> than <c> loop β values is in qualitative agreement that <a> loop dislocation densities are much larger than those of <c> loops.

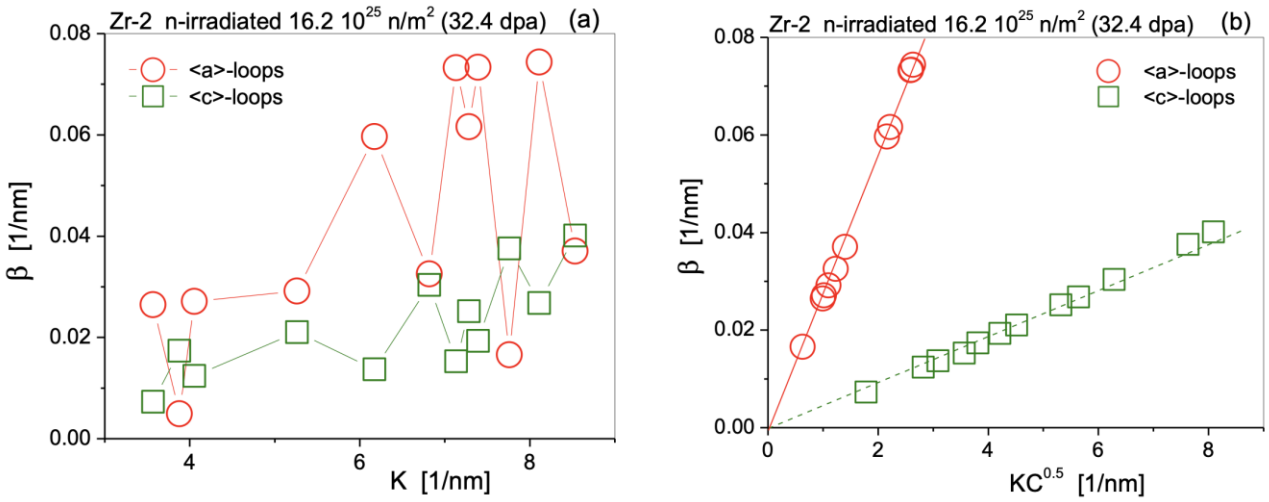

Figure 5. (a) Williamson-Hall plot of the integral breadth (β) values calculated from the theoretical diffraction patterns related to <a> (red circles) or <c> loops (green open squares). The plot shows that the FWHM values are in anticoincidence vs. K in correlation with the two related Burgers vectors almost normal to each other. (b) The same β values in the modified Williamson-Hall plot where K is scaled with the square root of the contrast factors, C. The large difference in the slopes of β vs. $K\sqrt{C}$ is in correlation with the large difference in the dislocation densities of <a>- and <c>- loops.

Dislocation density calculation with CMWP was carried out, using strain functions and contrast factors related to the <*a*>- and <*c*>-type loops. The dislocation densities of the <a>- and <c>- loop types in neutron irradiated Zircaloy-2 and Low-Sn ZIRLO are shown in Figure 6 (a) and (b) respectively, for five different fluences and the non-irradiated reference sample. In general, repeat measurements are within error of each other, except for an outlier denoted by an arrow in Figure 6 (b) and (d).

In the non-irradiated specimens, which are recrystallised, dislocation densities are smaller than 1×10^{14} m^{-2}. In the irradiated specimens, <a>-loop dislocation increases to the $\sim 50 \times 10^{14}$ m^{-2} for both samples at the lowest dose investigated. This value does not change significantly up to the highest dose, within the uncertainty of the measurements. However, the samples at 11.1×10^{25} n/m^2 have a dislocation density in the 10^{16} m^{-2} range consistently for all measurements for both alloys. The <c>-loop density is higher in Zircaloy-2 compared to low-Sn ZIRLO after 2.1×10^{25} n/m^2. There is a slight increase in <c>-loop dislocation density as a function of fluence for the Zircaloy-2 specimens, except for the single outlier with an anomalously large <c>-loop

dislocation density at 2.1 × 10^{25} n/m^2 (denoted by an arrow). The trend for the ZIRLO specimens is less clear.

Axial growth strain data from [12] for the same material is also plotted in Figure 6 (c). Low Sn ZIRLO shows favourable irradiation growth kinetics, compared to Zircaloy-2. At the highest dpa of 32.4 dpa, the axial growth of the Zircaloy-2 sample is 1.33%, compared to 0.43% in low Sn ZIRLO. This growth data is plotted directly against <c>-loop density in Figure 6 (d). Axial growth strain remains low, until <c>-loop density reaches 3 × 10^{14} m^{-2}, after which axial growth seems to be accompanied by marginal increase in <c>-loop line densities, except for the outlier denoted by an arrow.

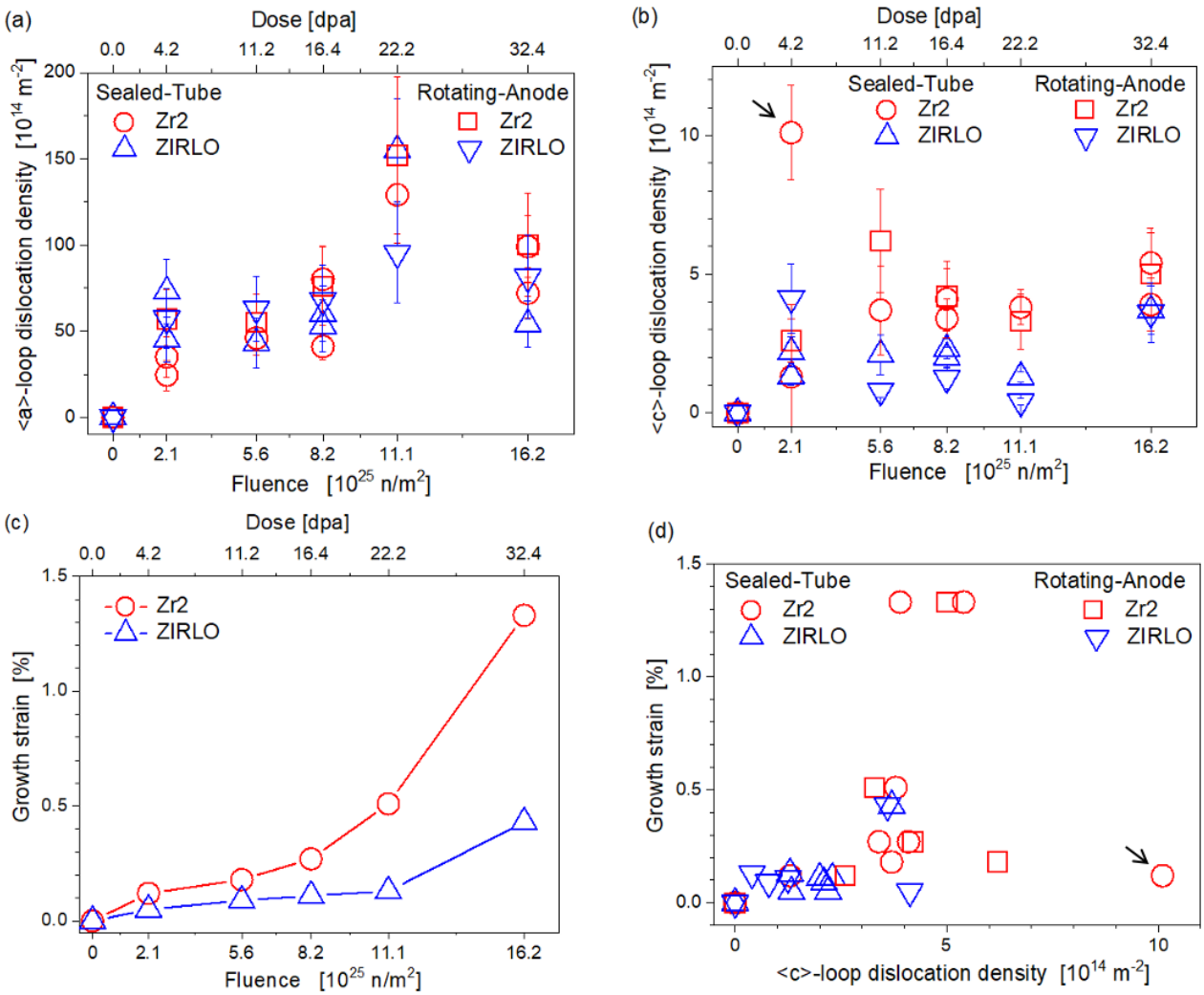

Figure 6. (a) Dislocation densities of (a) <a>-loop and (b) <c>-loops as a function of irradiation dose in both Zircaloy-2 (red symbols) and Low-Sn ZIRLO (blue symbols). (c)

Growth strain vs. neutron irradiation dose. (d) Growth strain vs. <c>-loop dislocation density. Growth strain data is published in [12].

Depth profiling of proton irradiated Zircaloy-4

Figure 7 (a) and (c) shows <a>-loop dislocation density as a function of depth for Zircaloy-4 samples irradiated to a nominal dose of 0.1 dpa and 2 dpa respectively. On the right-hand axis, the dose calculated from SRIM is also displayed. At depths over 30 μm, the dislocation density is smaller than 1×10^{14} m^{-2}, as is expected for a well recrystallised sample. This is consistent with the SRIM prediction where no dose, and therefore no irradiation damage, is expected beyond 30 μm.

The dislocation density and arrangement parameter profile for nominal doses of 0.1 and 2 dpa show different trends within the irradiated region (< 30 μm). It should be noted that within this region, the dose varies from around 0.5 times the nominal dose at 1 μm deep to 9 times the nominal at the Bragg peak at 30 μm deep. The dose rate is also variable in the irradiated region according to the same factors.

For the 0.1 dpa sample, the dislocation density is 3×10^{14} m^{-2} at a depth of 5 μm (corresponding to a dose of around 0.05 dpa) and increases to a peak of 55×10^{14} m^{-2} at a depth of 25 μm (corresponding to a dose of around 0.2 dpa). For the 2 dpa sample, the dislocation density profile is approximately constant at 20×10^{14} m^{-2} across the damaged region, from the surface to 30 μm. This is 2.75 times smaller than the peak dislocation density measured in the 0.1 dpa sample. Figure 7 (b) and (d) shows the <a> loop dislocation arrangement parameter as a function of depth for Zircaloy-4 samples irradiated to a nominal dose of 0.1 dpa and 2 dpa respectively. This parameter is not plotted where dislocation density is below 2×10^{14} m^{-2} as the parameter becomes unreliable for small dislocation densities.

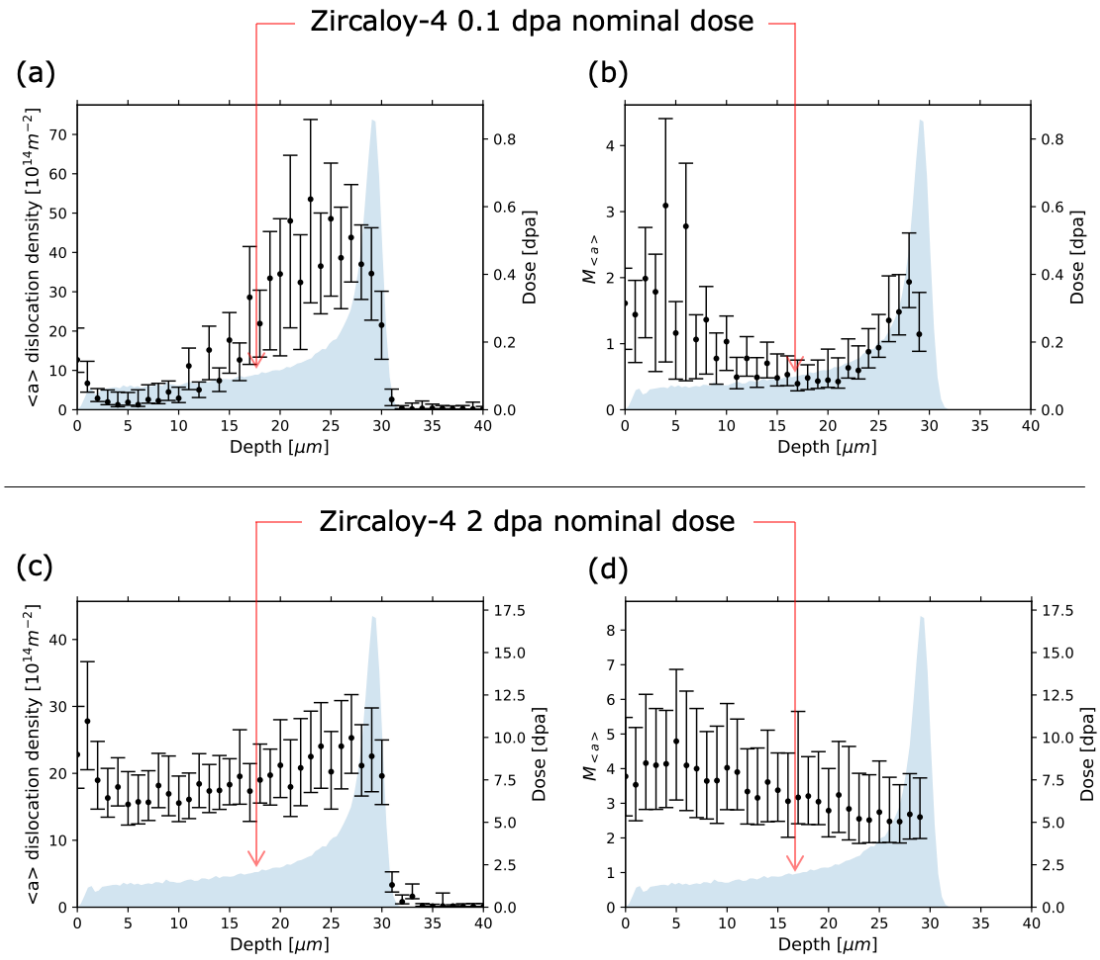

Figure 7. <a>-loop dislocation density as a function of depth for (a) 0.1 dpa and (c) 2 dpa Zirlocay-4 samples. <a>-loop dislocation arrangement parameter as a function of depth for (b) 0.1 dpa and (d) 2 dpa Zircaloy-4 samples. Dislocation arrangement parameter is only plotted where dislocation density is above 2 × 10^{14} m^{-2}. Dose as a function of depth, calculated using SRIM is also displayed by the light-blue shaded area.

The dislocation density and dislocation arrangement data are plotted in Figure 8 (a), (c) and (e), from samples at nominal doses of 0.1, 0.5, 1 and 2 dpa. This highlights the clear difference between the sample at a nominal dose of 0.1 dpa, and those at higher nominal dose. At a given depth, the dose rate in each sample is equivalent and these are marked in the plots. At the lowest dose rates, <a>-loop dislocation density increases as a function of dose, saturating at around 0.5 dpa. However, for the highest dose rate, dislocation density decreases as a function of dose, suggesting the annihilation of dislocation structures over time at temperature. For all dose rates, the dislocation arrangement parameter increases as a function of dose. The trend for <c>-

loop dislocation density is less clear, however for the 0.5, 1 and 2 dpa samples, there is an increase in dislocation density as a function of dose.

Dislocation density and dislocation arrangement parameter are directly plotted against predicted dose from SRIM in Figure 8 (b), (d) and (e). Datapoints from depths of between 5 and 25 μm are included, to remove effects from near the sample surface and to remain within the region where dose is more certain. Since each sample has a range of dose rates, points from equivalent depth in each sample, are connected by trendlines. Points connected by a solid line are from 25 μm depth corresponding to 2.6×10^{-5} dpa/s and points connected by a dashed line are from 5 μm depth corresponding to 0.8×10^{-5} dpa/s.

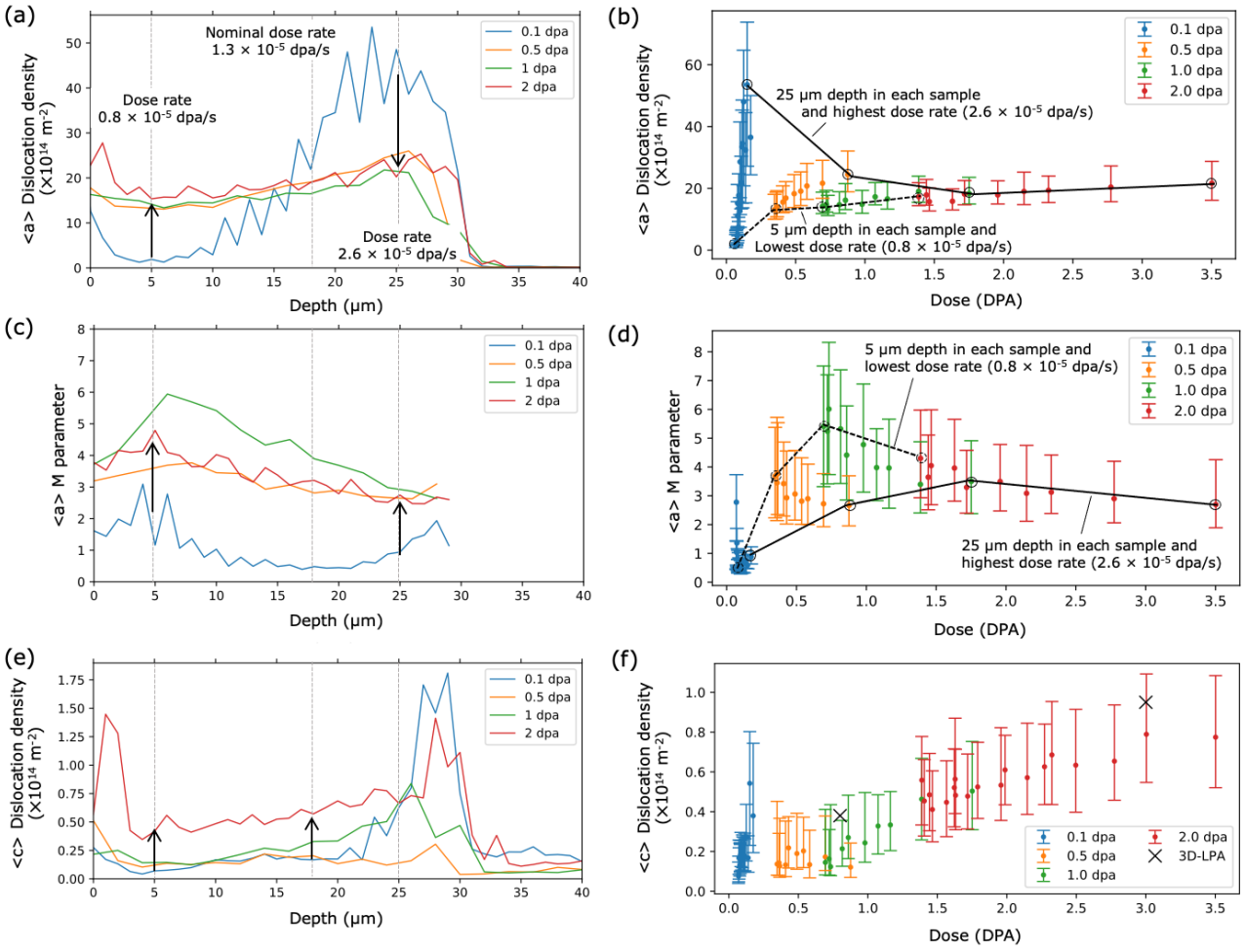

Figure 8. (a) <a>-loop dislocation density as a function of depth in Zircaloy-4 for nominal doses of 0.1, 0.5, 1.0 and 2.0 dpa. (b) Dislocation density as a function of predicted dose, plotted for all samples. (c) Dislocation arrangement parameter, M, as a function of depth,

plotted for each of the samples. (d) Dislocation arrangement parameter, M, as a function of predicted dose, plotted for all of the samples. (e) <c>-loop dislocation density as a function of depth in Zircaloy-4 for each sample. (f) <c>-loop dislocation density as a function of predicted dose, plotted for all samples. Black trend lines in (b) and (d) denote highest and lowest dose datapoints from each sample.

Grain resolved dislocation measurement

Total dislocation density as a function of depth, for each individual grain in the Zr-0.1Fe material studied, is plotted in Figure 9 (a) and (b) for the 0.8 dpa and the 3 dpa samples respectively. The grain average dislocation density (including all loop types) is 4.2 ± 2.0 × 10^{14} m^{-2} and 3.2 ± 1.8 × 10^{14} m^{-2} in the 0.8 dpa and 3 dpa samples respectively. Errors here are quoted as the standard deviation. The distribution of dislocation densities for each grain is also shown as a histogram to the right of Figure 9 (a) and (b).

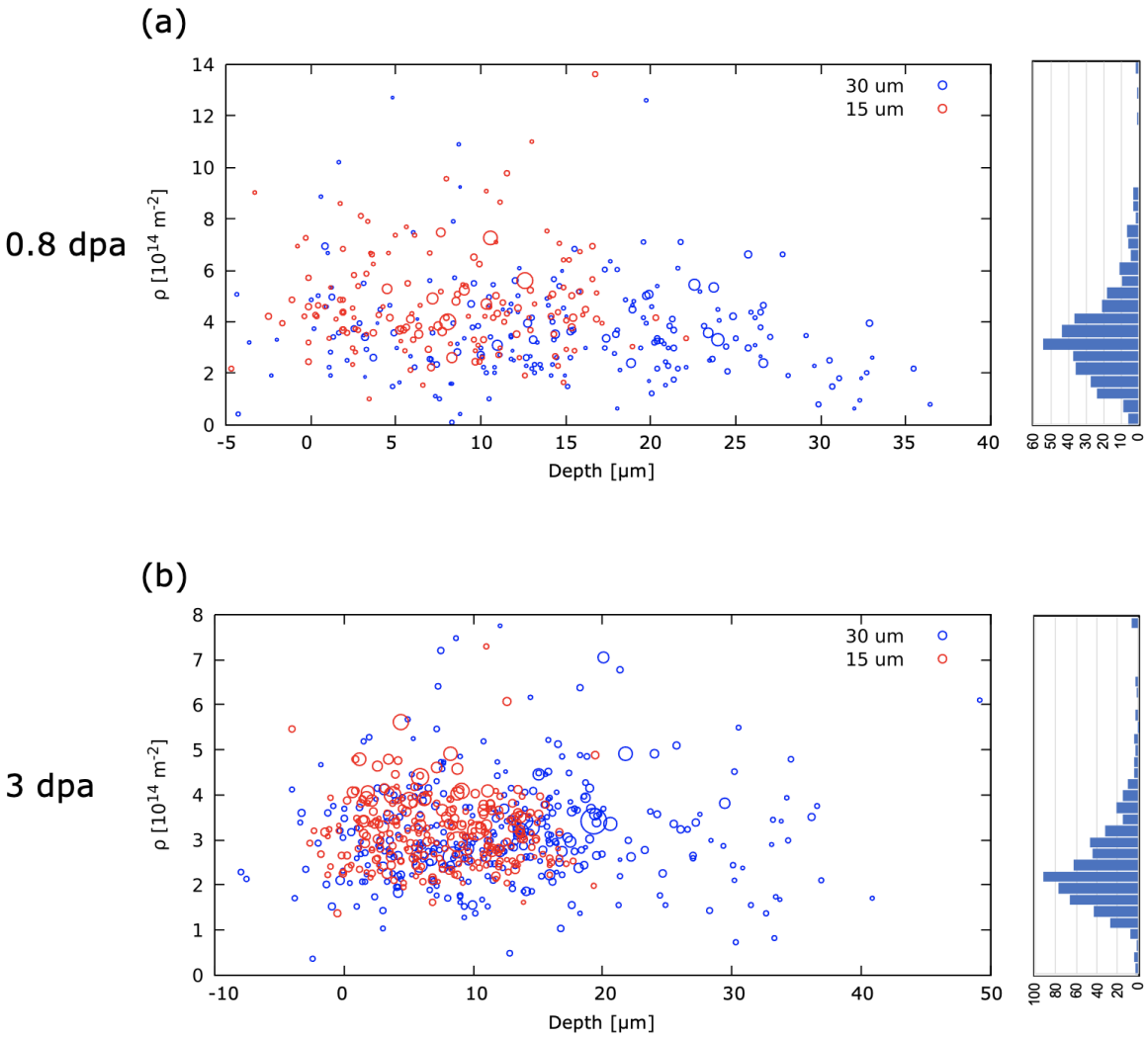

Figure 9. Dislocation density in each individual grain as a function of depth away from the proton irradiated surface of the Zr-0.1Fe material, for the (a) 0.8 and (c) 3 dpa samples. Circle diameter is proportional to grain volume to power 1/3 and colour represents the portion of the sample from which the data was obtained. Histograms of dislocation density are shown to the right.

Since individual grain diffraction patterns are collected, patterns are obtained for each signed hkl reflection. In the case of powder diffraction this is not the case since only the lengths of the diffraction vectors are registered while their diffractions merge as an average to form the Debye-Scherrer rings. Since the contrast factor is different for each signed reflection, loop type can be determined in the case of grain resolved 3D-LPA measurements. The loop types considered are shown in Table 3 and are based on [8]. The majority of the dislocation density in both the 0.8 and 3 dpa sample is attributed to the two loop types highlighted in green in Table 3. That is, 1/3 <11-20> [10-10]

<a>-loops and 1/6 <20-23> [0001] <c>-loops. Note that <c>-loops are not pure <c> type but are rather technically <c+a> loops. They are referred to as <c>-loops for consistency with literature. Small amounts of 1/3 <11-20> [11-20] and <10-10> [10-10] dislocations were also measured, but an order of magnitude less than 1/3 <11-20> [10-10]. The average 1/6 <20-23> [0001] <c>-loop dislocation density increases from 0.38 × 10^{14} m^{-2} in the 0.8 dpa sample to 0.95 × 10^{14} m^{-2} in the 3 dpa sample. This is consistent with the values measured from the depth profiling study, see Figure 8 (f).

Table 3. Loop types considered during analysis of 3D-LPA data and grain average dislocation density of each loop type, for both doses of the Zr-0.1Fe samples.

Loop Burgers vector and habit plane	Loop type	Average dislocation density per grain in 0.8 dpa sample (× 10^{14} m^{-2})	Average dislocation density per grain in 3.0 dpa sample (× 10^{14} m^{-2})
1/3 <11-20> [11-20]	<a>	0.37	0.19
1/3 <11-20> [10-10]	<a>	3.09	2.15
<10-10> [10-10]	<a>	0.27	0.25
1/3 <11-23> [10-11]	<c>	0.05	0.05
1/3 <11-23> [10-12]	<c>	0.02	0.02
1/6 <20-23> [0001]	<c>	0.38	0.95

As well as grain position, the crystallographic orientation of each grain can also be determined. Total dislocation density as a function of orientation, for each grain, plotted on an inverse pole figure (IPF), are shown in Figure 10 (a) and (b) for the 0.8 dpa and 3 dpa samples respectively. Dislocation density against the declination angle of the c-axis away from the irradiation direction are shown in Figure 10 (c) and (d) for the 0.8 dpa and 3 dpa samples respectively. There is no clear trend of dislocation density as a function of crystallographic orientation observed in either the IPF or the declination angle plots. Although not plotted here, dislocation density as a function of grain size was also investigated and again, no trend was observed.

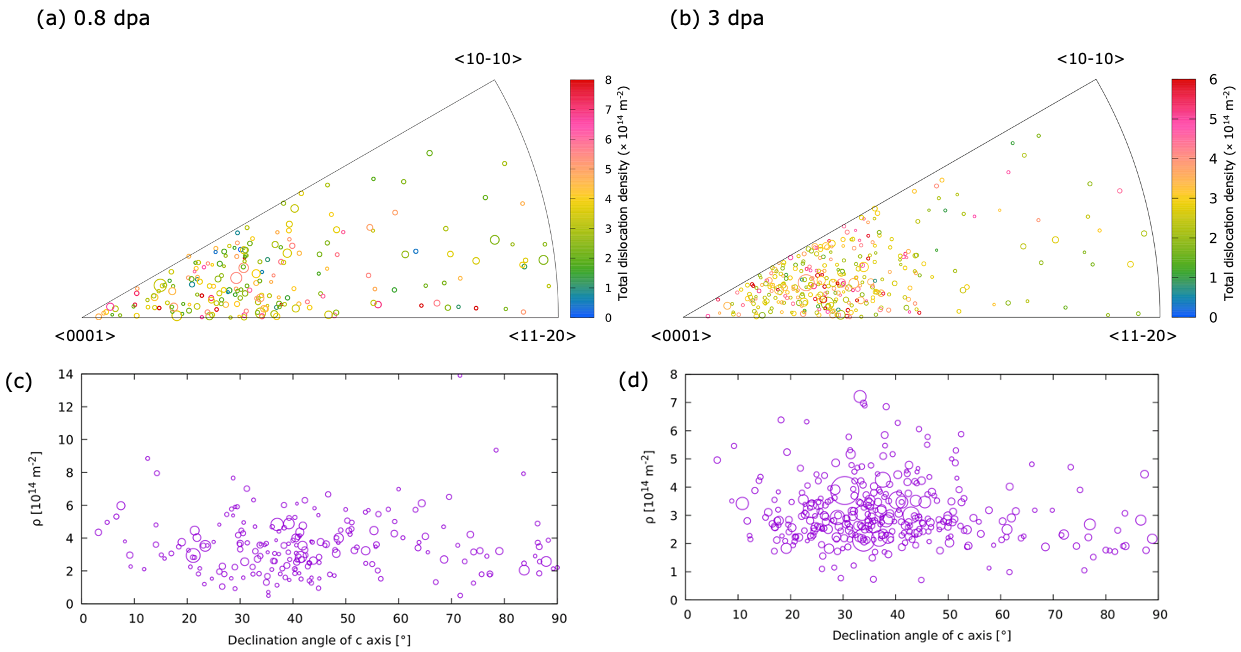

Figure 10. (a-b) Inverse pole figure of irradiation direction for each grain in the 0.8 dpa sample and 3 dpa sample respectively, in the Zr-0.1 Fe samples, where colour represents total dislocation density. Circle diameter is proportional to grain volume to power 1/3. (c-d) Total dislocation density as a function of declination angle of c-axis away from the irradiation direction for each grain in the 0.8 dpa and 3 dpa samples respectively.

4. Discussion

Bulk measurement of BOR-60 samples

To improve the performance of cladding tubes, understanding the relationship between alloy composition, irradiation damage structures and resultant irradiation growth is crucial. The key focus of the BOR-60 study was the accurate quantification of <a>-loop and <c>-loop dislocation density, for a systematic range of alloys and doses, and subsequent correlation to axial irradiation growth measured on the same material by Yagnik et al. [12]. Axial growth strain remains low (< 0.2%) until a <c>-loop dislocation density of ~3 × 10^{14} m^{-2} is reached, after which the correlation becomes less clear. Therefore, with the data available in the current study, only a weak correlation of breakaway axial growth strain with <c>-loop dislocation density can be reported. A clearer correlation between axial growth strain and average <c>-loop density measured by TEM, was observed by Yagnik et al. [12]. Due to various factors, including difficulty

in quantification of microscopy and <c>-loop diameters exceeding the foil thickness, it was noted that <c>-loop densities measured by TEM were likely to be an underestimate. The average <c>-loop density in RXA Zircaloy-2 at a fluence of 16.2 × 10^{25} n/m^2, was measured by TEM in [12] to be ~ 1.7 × 10^{14} m^{-2} compared to 4.8 × 10^{14} m^{-2} in the current study (taken to be the mean of all 3 measurements). At the lowest fluence of 2.1 × 10^{25} n/m^2, the <c>-loop density was measured by TEM in [12] to be ~ 0.2 × 10^{14} m^{-2} compared to 2.0 × 10^{14} m^{-2} in the current study (taken to be the mean of 2 measurements, excluding an apparent outlier at 10.1 × 10^{14} m^{-2}). This apparent outlier was taken from another side of the sample, compared to the other measurements taken on the same sample. This suggests a possible sample preparation issue, even though both sides of the sample were electropolished simultaneously. The difference between TEM and XRD-LPA is more pronounced at lower dose (where there is factor of about 10) compared to higher dose (where there is a factor of about 2). This could be either due to small <c>-component features which are not seen in TEM (as discussed in [6] and may help explain the formation and evolution of <c>-loops), or perhaps large loops which exceed the foil thickness.

Dislocation density has also been measured on neutron-irradiated RXA Zircaloy-2 by Seymour et al. [4] on cladding irradiated at ~ 350 °C and channel material irradiated at ~ 300 °C. <a>-loop dislocation densities measured in the current study are in good agreement are within the bounds of values measured by line profile analysis in [4] and are closer to values for channel material as opposed to cladding. <c>-loop dislocation densities measured in the current study are also in close agreement with values measured by line profile analysis in [4], which are similar for both channel material and cladding.

Further measurements are ongoing, and these results will be presented at a later date. Further TEM of the BOR-60 samples is also in progress, and this will be shared at a later date to complement the XRD measured dislocation density. Furthermore, chemical mapping, both in the TEM and with atom probe tomography will be used to investigate the link between chemical segregation and irradiation induced dislocation loop formation.

Depth profiling of proton irradiated Zircaloy-4

The depth profiling experiments on proton-irradiated Zircaloy-4 samples show clear agreement of experimental results with the extent of the irradiated region predicted by SRIM. The integral irradiation dose of 2 MeV protons into zirconium was expected to be contained within a depth of 30 μm and this was indeed the case in experimental measurements, to within 1 μm. As a result, previous assumptions made about depths from which to extract TEM foils as to remain are correct. Generally, a depth of ~ 18 μm is targeted, such that the dose throughout the foil thickness is constant. Even with some uncertainty of the exact depth from which the foil is extracted, the dose is fairly constant. For example, within ± 2 μm of 18 μm depth, the dose (and therefore dose rate) remains within ± 10%. However, it should be noted that the resulting irradiation damage is variable at low nominal dose.

At a nominal dose of 0.1 dpa, both dislocation density and dislocation arrangement parameter vary strongly as a function of depth, therefore also as a function of dose and dose rate. Care should therefore be taken when performing microscopy on low dose samples since the dislocation structure is not constant, even near the region where dose and dose rate are approximately constant, up to around 20 μm depth. At nominal doses of 0.5 dpa up to 2 dpa, an increasingly flat damage profile is observed. This suggests, at least for lower dose rates, that dislocation density saturates as a function of dose, as shown by the dotted line in in Figure 8 (b). This is in agreement with previous observations by Seymour et al. [4], which show a plateau in peak FWHM of neutron irradiated Zircaloy-2, for fluences between 9 - 15 × 10^{25} n/m^2. A limitation of neutron irradiated material, however, is that the doses are typically high and the behaviour at low doses is missed. The current study captures the behaviour at comparatively small doses. The saturation in <a>-loop dislocation density is also reflected in mechanical properties, specifically ultimate tensile strength (UTS), in a number of studies [25–27].

For higher dose rate, near the Bragg peak, the dislocation density decreases as a function of dose, as shown by the solid line in in Figure 8 (b). This suggests that annihilation of dislocation structures or loop size growth may be occurring in this region. As shown previously by Topping et al. [2], dislocation arrangement parameter is loosely related to dislocation loop size. Assuming this relationship holds true here also, <a>-loop size might be increasing as a function of dose. The effect of dose rate is less

significant for higher doses, with both dashed and solid curves converging in Figure 8 (b).

At 3.5 dpa in the proton-irradiated RXA Zircaloy-4, the dislocation density was measured to be 22 ± 6 × 10^{14} m^{-2}. At the lowest BOR-60 dose of 4.2 dpa, the dislocation density in the RXA Zircaloy-2 sample was measured to be 33 ± 10 × 10^{14} m^{-2}. These values are within uncertainty of each other and therefore the depth profiling measurements are consistent with the bulk measurements performed on neutron irradiated BOR-60 samples. The difference between the two measurements is likely attributed to the small difference in alloy chemistry between Zircaloy-2 and Zircaloy-4 and the effect of protons vs neutrons and the associated conversion factor, temperature and dose rate differences.

Further depth profiling measurements at doses lower than 0.1 dpa would give further insight into the early stages of <a>-loops nucleation. Also, since there remains a gap between the doses investigated with proton and neutron irradiation, depth profiling on samples proton-irradiated to higher doses would be beneficial to further compare the irradiation structures produced by both techniques. The <c>-loop content of the samples investigated here is low, even near the Bragg peak in the high dose sample. Therefore, irradiating samples to doses higher than 2 dpa would be beneficial to systematically investigate <c>-loop nucleation and growth and the relationship between <a>- and <c>-loops. Furthermore, the depth-profiling method described in this paper has the possibility to probe other heterogeneous nuclear microstructures, such as other types of ion irradiations, coatings for accident tolerance and the effect of processing on cladding tubes.

Grain-resolved dislocation measurement

Isolating diffraction spots for individual grains and reconstructing the line profile for each grain allows grain-to-grain variability in physical parameters such as dislocation density, dislocation arrangement parameter and lattice parameter to be measured. At both nominal doses investigated here, there exists a broad variability in dislocation density, which is important to note for TEM studies, which generally investigate only a few grains. Nonetheless, an increase in <c>-loop dislocation density was observed from 0.8 dpa to 3 dpa. The dislocation densities measured in the grain-resolved experiment

are also lower than those measured in the bulk and depth profiling measurements. This could be due to the different alloy compositions used for each experiment.

Channelling is one possible reason for grain-to-grain variability in dislocation density, whereby the crystal orientation relative to the irradiation direction may impact energy deposition and implantation range [11]. This is particularly important to study, since TEM studies of <a>-loops in electropolished foils are constrained to investigate a subset of grains where the [11-20] crystal orientation is parallel with the TEM foil normal [11]. In the current study, no trend was observed between crystallographic orientation and dislocation density. However, due to the texture of the material and the chosen irradiation direction, there is a lack of data around [11-20] and [10-10] poles. It should be noted that crystal orientation is unlikely to have an effect on energy deposition in neutron irradiated samples [11].

Almost all <a>-loop dislocation density in the current study was attributed to 1/3 <11-20> [10-10] type loops. The observed Burgers vector is consistent with previous observations by Northwood et al. [28], where only loops with a 1/3 <11-20> Burgers vector were observed. Both Jotsons et al. [29] and Kelly et al. [30] conclude that dislocation loops prefer the [10-10] habit plane. However, in most cases it was determined to be a mixture between [10-10] and [11-20], with a small shift towards [0001]. It should be noted that a limitation of line profile analysis is that only the dislocation loop habit plane and Burgers vector combinations provided to the software can be measured. Therefore, TEM is necessary to find the predominant loop types in the first instance, then line profile analysis provides a robust quantification.

Almost all <c>-loop dislocation density in the current study was attributed to 1/6 <20-23> [0001] type loops. A review by Griffiths [1] also concluded that most irradiation-induced <c>-component dislocation are loops on the basal plane with Burgers vector 1/6 <20-23>. Since large <c>-loops in neutron irradiated material exhibit weak diffraction contrast, observation in TEM is particularly challenging and line profile analysis therefore provides a complementary alternative.

In terms of zirconium alloys, grain resolved dislocation density measurement has so far only been carried out on proton-irradiated Zr-Fe binary samples at two doses. It is planned to measure Zircaloy-4 samples proton irradiated to 0.1 dpa, then deformed in

tension, as described in [31]. The aim will be to investigate the evolution of both dislocation loops and deformation-induced dislocations as a function of deformation. Depending on grain orientation, deformation will occur on different slip systems and therefore may have different channel clearing behaviours. In principle, neutron-irradiated samples, such as the BOR-60 samples discussed previously could also be studied. Although no orientation dependence might be expected in neutron-irradiated samples, the evolution of loop type and grain-to-grain variability could be investigated in such samples.

5. Conclusions

Line profile analysis of bulk samples with a laboratory diffractometer has been shown to give complementary information to microscopy. Novel depth profiling at a synchrotron gives information about a range of doses and dose rates in a single sample, enabling systematic studies. Grain-resolved line profile analysis experiments at a synchrotron give further insight into dislocation structures on a grain-by-grain basis. The key findings from the studies are as follows:

- With the data available in the current study, only a weak correlation of breakaway axial growth strain with <c>-loop dislocation density can be reported
- Dislocation density of <c>-loops, measured by line profile analysis, are larger than values published in literature measured by TEM by a factor of ~2-10, suggesting there may be <c>-component features which are not seen in TEM, or large loops which exceed the foil thickness.
- The extent of the damaged region in Zircaloy-4 irradiated with 2 MeV protons is consistent with prediction from simulation. For doses less than 0.1 dpa, a variable irradiation damage profile is observed as a function of depth, whereas increasingly flat dislocation density profile is observed for higher doses.
- There exists a grain-to-grain dislocation density variability in proton-irradiated Zr-0.1Fe, however no trend between dislocation density and crystallographic orientation relative to the irradiation direction was observed, suggesting that channelling is not significant for the crystallographic orientations sampled.

- Mostly, <11-20> [10-10] <a>-loops and <20-23> [0001] <c>-loops were observed, with all other loop types having an order of magnitude lower dislocation densities.

6. Acknowledgments

The authors would like to thank Matthew Topping, Alistair Garner, Albert Smith, Hattie Xu and Sheng Cao for their assistance with synchrotron experiments and data analysis. The BOR-60 samples were provided by the EPRI-led NFIR programme. The authors would like to thank the Engineering and Physical Sciences Research Council UK for funding the study through the MIDAS (Mechanistic understanding of Irradiation Damage in fuel ASsemblies) programme grant (EP/S01702X/1). We acknowledge DESY (Hamburg, Germany), a member of the Helmholtz Association HGF, for the provision of experimental facilities. This research used resources of the Advanced Photon Source, a U.S. Department of Energy (DOE) Office of Science user facility operated for the DOE Office of Science by Argonne National Laboratory under Contract No. DE-AC02-06CH11357. The research used UKAEA's Materials Research Facility, which has been funded by and is part of the UK's National Nuclear User Facility and Henry Royce Institute for Advanced Materials. This work has been part-funded by the EPSRC Energy Programme grant number EP/T012250/1. G.R. is grateful for the support of OTKA grant K124926 funded by the Hungarian National Research, Development and Innovation Office (NKFIH).

7. References

[1] M. Griffiths, A review of microstructure evolution in zirconium alloys during irradiation, J. Nucl. Mater. 159 (1988) 190–218. https://doi.org/10.1016/0022-3115(88)90093-1

[2] M. Topping, A. Harte, T. Ungár, C.P. Race, S. Dumbill, P. Frankel, M. Preuss, The effect of irradiation temperature on damage structures in proton-irradiated zirconium alloys, J. Nucl. Mater. 514 (2019) 358–367. https://doi.org/10.1016/j.jnucmat.2018.12.006

[3] T. Ungar, G. Ribarik, M. Topping, R.M.A. Jones, X.D. Xu, R. Hulse, A. Harte, G. Tichy, C.P. Race, P. Frankel, M. Preuss, Characterizing dislocation loops in irradiated polycrystalline Zr alloys by X-ray line profile analysis of powder diffraction patterns with satellites, J. Appl. Crystallogr. 54 (2021) 803–821. https://doi.org/10.1107/S1600576721002673

[4] T. Seymour, P. Frankel, L. Balogh, T. Ungár, S.P. Thompson, D. Jädernäs, J. Romero, L. Hallstadius, M.R. Daymond, G. Ribárik, M. Preuss, Evolution of dislocation structure in neutron irradiated Zircaloy-2 studied by synchrotron x-ray diffraction peak profile analysis, Acta Mater. 126 (2017) 102–113. https://doi.org/10.1016/j.actamat.2016.12.031

[5] M. Topping, T. Ungár, C.P. Race, A. Harte, A. Garner, F. Baxter, S. Dumbill, P. Frankel, M. Preuss, Investigating the thermal stability of irradiation-induced damage in a zirconium alloy with novel in situ techniques, Acta Mater. 145 (2018) 255–263. https://doi.org/10.1016/j.actamat.2017.11.051

[6] T. Ungár, P. Frankel, G. Ribárik, C.P. Race, M. Preuss, Size-distribution of irradiation-induced dislocation-loops in materials used in the nuclear industry, J. Nucl. Mater. 550 (2021) https://doi.org/10.1016/j.jnucmat.2021.152945

[7] L. Balogh, D.W. Brown, P. Mosbrucker, F. Long, M.R. Daymond, Dislocation structure evolution induced by irradiation and plastic deformation in the Zr-2.5Nb nuclear structural material determined by neutron diffraction line profile analysis, Acta Mater. 60 (2012) 5567–5577. https://doi.org/10.1016/j.actamat.2012.06.062

[8] L. Balogh, F. Long, M.R. Daymond, Contrast factors of irradiation-induced dislocation loops in hexagonal materials, J. Appl. Crystallogr. 49 (2016) 2184–2200. https://doi.org/10.1107/S1600576716018136

[9] A. Harte, M. Topping, P. Frankel, D. Jädernäs, J. Romero, L. Hallstadius, E.C. Darby, M.Preuss, Nano-scale chemical evolution in a proton-and neutron-irradiated Zr alloy, J. Nucl. Mater. 487 (2017) 30–42. https://doi.org/10.1016/j.jnucmat.2017.01.049

[10] R.B. Adamson, C.E. Coleman, M. Griffiths, Irradiation creep and growth of zirconium alloys: A critical review, J. Nucl. Mater. 521 (2019) 167–244. https://doi.org/10.1016/j.jnucmat.2019.04.021

[11] A. Adrych-Brunning, C.P. Race, The interaction of proton irradiation with Zr textured microstructure, J. Nucl. Mater. 547 (2021) https://doi.org/10.1016/j.jnucmat.2021.152808

[12] S. Yagnik, R.B. Adamson, G. Kobylyansky, J.H. Chen, D. Gilbon, S. Ishimoto, T. Fukuda, L. Hallstadius, A. Obukhov, S. Mahmood, Effect of alloying elements, cold work, and hydrogen on the irradiation-induced growth behavior of zirconium alloy variants, ASTM Spec. Tech. Publ. STP 1597 (2018) 748–795. https://doi.org/10.1520/STP159720160040

[13] L. Walters, S.R. Douglas, M. Griffiths, Equivalent radiation damage in zirconium irradiated in various reactors, ASTM Spec. Tech. Publ. STP 1597 (2018) 676–690. https://doi.org/10.1520/STP159720160101

[14] R.E. Stoller, M.B. Toloczko, G.S. Was, A.G. Certain, S. Dwaraknath, F.A. Garner, On the use of SRIM for computing radiation damage exposure, Nucl. Instruments Methods Phys. Res. Sect. B Beam Interact. with Mater. Atoms. 310 (2013) 75–80. https://doi.org/10.1016/j.nimb.2013.05.008

[15] J.F. Ziegler, M.D. Ziegler, J.P. Biersack, SRIM - The stopping and range of ions in matter (2010), Nucl. Instruments Methods Phys. Res. Sect. B Beam Interact. with Mater. Atoms. 268 (2010) 1818–1823. https://doi.org/10.1016/j.nimb.2010.02.091

[16] ASTM, Designation E521 – 16, Standard Practice for Investigating the Effects of Neutron Radiation Damage Using Charged-Particle Irradiation, 96 (2017) 1–21. https://doi.org/10.1520/E0521-16

[17] T. Ungár, G. Ribárik, G. Zilahi, R. Mulay, U. Lienert, L. Balogh, S. Agnew, Slip systems and dislocation densities in individual grains of polycrystalline aggregates of plastically deformed CoTi and CoZr alloys, Acta Mater. 71 (2014) 264–282. https://doi.org/10.1016/j.actamat.2014.03.024

[18] B.E. Warren, X-ray studies of deformed metals, Prog. Met. Phys. 8 (1959) 147–

202. https://doi.org/10.1016/0502-8205(59)90015-2
[19] T. Ungár, I. Dragomir, Á. Révész, A. Borbély, The contrast factors of dislocations in cubic crystals: The dislocation model of strain anisotropy in practice, J. Appl. Crystallogr. 32 (1999) 992–1002. https://doi.org/10.1107/S0021889899009334
[20] G. Ribárik, B. Jóni, T. Ungár, Global optimum of microstructure parameters in the CMWP line-profile-analysis method by combining Marquardt-Levenberg and Monte-Carlo procedures, J. Mater. Sci. Technol. 35 (2019) 1508–1514. https://doi.org/10.1016/j.jmst.2019.01.014
[21] M.A. Krivoglaz, X-Ray and Neutron Diffraction in Nonideal Crystals, 1st editio, Springer Berlin Heidelberg, Berlin, Heidelberg, 1996
[22] M. Wilkens, Fundamental Aspects of Dislocation Theory, in: J.A. Simmons, R. Bullough, R. DeWit (Eds.), 2nd ed., National Bureau of Standards (US) Special Publication, 1970: pp. 1195–1221
[23] T. Ungár, G. Ribárik, L. Balogh, R. Thomas, O. Koc, C.P. Race, M. Preuss, P. Frankel, Partial dislocation densities of dislocation loops and lattice dislocations in neutron or proton irradiated Zr alloys, in preparation, (n.d.)
[24] G. Ribárik, B. Jóni, T. Ungár, The Convolutional Multiple Whole Profile (CMWP) Fitting Method, a Global Optimization Procedure for Microstructure Determination, Crystals. 10 (2020) 623. https://doi.org/10.3390/cryst10070623
[25] B. V. Cockeram, K.J. Leonard, T.S. Byun, L.L. Snead, J.L. Hollenbeck, Development of microstructure and irradiation hardening of Zircaloy during low dose neutron irradiation at nominally 377-440 °C, J. Nucl. Mater. 449 (2014) 69–87. https://doi.org/10.1016/j.jnucmat.2014.03.004
[26] B. V. Cockeram, R.W. Smith, K.J. Leonard, T.S. Byun, L.L. Snead, Development of microstructure and irradiation hardening of Zircaloy during low dose neutron irradiation at nominally 358°C, J. Nucl. Mater. 418 (2011) 46–61. https://doi.org/10.1016/j.jnucmat.2011.07.006
[27] K. Farrell, T.S. Byun, N. Hashimoto, Deformation mode maps for tensile deformation of neutron-irradiated structural alloys, J. Nucl. Mater. 335 (2004) 471–486. https://doi.org/10.1016/j.jnucmat.2004.08.006
[28] D.O. Northwood, R.W. Gilbert, L.E. Bahen, P.M. Kelly, R.G. Blake, A. Jostsons, P.K. Madden, D. Faulkner, W. Bell, R.B. Adamson, Characterization of neutron irradiation damage in zirconium alloys - an international "round-robin" experiment, J. Nucl. Mater. 79 (1979) 379–394. https://doi.org/10.1016/0022-

3115(79)90103-X

[29] A. Jostsons, P.M. Kelly, R.G. Blake, The nature of dislocation loops in neutron irradiated zirconium, J. Nucl. Mater. 66 (1977) 236–256. https://doi.org/10.1016/0022-3115(77)90113-1

[30] P.M. Kelly, R.G. Blake, The Characterization of Dislocation Loops in Neutron irradiated Zirconium, Philos. Mag. 28 (1973) 415–426. https://doi.org/10.1080/14786437308217463

[31] R. Thomas, D. Lunt, M.D. Atkinson, J. Quinta da Fonseca, M. Preuss, F. Barton, J. O'Hanlon, P. Frankel, The effect of loading direction on slip and twinning in an irradiated zirconium alloy, Zircon. Nucl. Ind. Ninet. Int. Symp. (2020) https://doi.org/10.1520/STP162220190027